JOURNAL OF NEUROTRAUMA 32:1158–1167 (August 1, 2015)

DOI: 10.1089/neu.2014.3703

Fibronectin Matrix Assembly after Spinal Cord Injury

Yunjiao Zhu, Cynthia Soderblom, Michelle Trojanowsky, Do-Hun Lee, and Jae K. Lee

Abstract

After spinal cord injury (SCI), a fibrotic scar forms at the injury site that is best characterized by the accumulation of perivascular fibroblasts and deposition of the extracellular matrix protein fibronectin. While fibronectin is a growth-permissive substrate for axons, the fibrotic scar is inhibitory to axon regeneration. The mechanism behind how fibronectin contributes to the inhibitory environment and how the fibronectin matrix is assembled in the fibrotic scar is unknown. By deleting fibronectin in myeloid cells, we demonstrate that fibroblasts are most likely the major source of fibronectin in the fibrotic scar. In addition, we demonstrate that fibronectin is initially present in a soluble form and is assembled into a matrix at 7 d post-SCI. Assembly of the fibronectin matrix may be mediated by the canonical fibronectin receptor, integrin $\alpha5\beta1$, which is primarily expressed by activated macrophages/microglia in the fibrotic scar. Despite the pronounced cavitation after rat SCI, fibrotic scar also is observed in a rat SCI model, which is considered to be more similar to human pathology. Taken together, our study provides insight into the mechanism of fibrotic scar formation after spinal cord injury.

Key words: fibronectin; fibrotic scar; macrophages; microglia; spinal cord injury

Introduction

After spinal cord injury (SCI), a scar tissue forms at the injury site that comprises glial and fibrotic components. The glial scar is characterized by extensive astrogliosis surrounding the central core region of the injury site. The fibrotic scar occupies the injury core and is made up of fibroblasts and a dense extracellular matrix (ECM). The scar tissue not only plays a protective role by limiting spreading of inflammation and secondary damage to nearby intact tissue, but it also serves as an inhibitory barrier for axon regeneration.[1,2] Recent studies of the scar tissue have been mostly focused on the glial scar while the fibrotic component has received less attention. In vitro models of the scar tissue using co-culture of astrocytes and meningeal fibroblasts show that the fibrotic scar is inhibitory for axon growth.[3–5] In vivo ablation of fibroblasts after SCI lead to compromised tissue integrity and cavitation at injury site.[6] Thus, understanding how the fibrotic scar is formed may provide novel insights into SCI pathology.

The fibrotic scar has traditionally been described as areas with high fibronectin immunoreactivity.[7,8] While fibronectin is not expressed at high levels in the normal adult spinal cord, previous studies suggest that its excess deposition after SCI could come from multiple sources, such as reactive astrocytes, macrophages, and fibroblasts.[9–11] In addition to serving as a scaffold to which many other extracellular matrix molecules can bind, fibronectin is known to be involved in many cellular functions, including migration, proliferation, and differentiation.[12–14] Fibronectin is expressed by a single gene with multiple isoforms generated by alternative splicing—the two major types being plasma and cellular fibronectin. Plasma fibronectin is produced by liver hepatocytes and released into the blood where it functions in forming a provisional blood clot that allows cells to migrate into the injury site and perform tissue remodeling for wound repair. During this process, the provisional clot, along with plasma fibronectin, is degraded by infiltrating cells expressing many different isoforms of cellular fibronectin that is assembled into a more stable matrix.

To be a functional matrix, fibronectin needs to polymerize into a fibrillar network, which is initiated by binding to cellular integrin receptors. Upon binding to fibronectin, integrin receptors cluster and bring adjacent fibronectin fibrils close together, thereby promoting their association and formation into a matrix.[11] However, whether or how this fibronectin matrix assembly occurs after SCI is not known.

Penetrating SCI in humans that disrupts dura mater often leads to invasion of meningeal fibroblasts and deposition of a fibrous connective tissue in the lesion core. This is similar to penetrating SCI in mice, as we described previously.[15] However, the most prevalent type of SCI in human patients is contusion, in which the dura remains largely intact and the lesion core often develops fluid-filled cavities.[16,17] Using a mouse model of contusive SCI, we demonstrated that perivascular fibroblasts detach from blood vessels and form a compact fibrotic scar at the injury site.[15] However, the extent to which this fibrotic scar also is conserved across species is not known, especially in rats that exhibit a similar pathology to human patients with contusive SCI.

In this study, we demonstrate that fibronectin is assembled into a matrix to form the fibrotic scar and this process is likely mediated by the fibronectin receptor integrin $\alpha5\beta1$, which is primarily expressed by activated macrophages/microglia. We also show that

Department of Neurological Surgery, Miami Project to Cure Paralysis, University of Miami School of Medicine, Miami, Florida.

deletion of fibronectin in myeloid cells does not change fibronectin expression level, indicating that fibroblasts are likely the major source of fibronectin in the fibrotic scar. Finally, we demonstrate the presence of fibrotic markers in a move translational rat contusion model, highlighting the clinical relevance of the fibrotic scar. Overall, our study provides novel insight into the mechanism of fibrotic scar formation after SCI.

Methods

Animals

For our study, lysM-Cre (#004781) mice were obtained from Jackson Labs (Bar Harbor, ME). Col1α1-GFP mice were kindly donated by Dr. David Brenner.[18] Rosa26-tdTomato reporter mice were kindly donated by Dr. Fan Wang.[19] Floxed fibronectin (FN) mice were kindly donated by Dr. Sakai Takao.[20] All mice were backcrossed to C57BL/6 for at least six generations. The lysM-Cre mice were bred to Rosa26-tdTomato reporter mice to generate lysM^{tdTom} in which lysM-Cre is hemizygous and tdTomato is homozygous. The same strategy was used to generate lysM-FN$^{fl/fl}$ mice. Sprague-Dawley rats were obtained from Harlan Laboratories (Dublin, VA).

Surgery and behavioral assessment

Eight- to ten-week-old female mice were anesthetized (ketamine/xylazine, 100 mg/15 mg/kg intraperitoneally) before receiving midthoracic (T8) contusive spinal cord injuries. Mice received a laminectomy at T8, then the spinal column was stabilized using spinal clamps and positioned on an Infinite Horizon impactor device (Precision Systems and Instrumentation, Lexington, KY). The exposed spinal cord was visually aligned with the impactor tip and given a moderate (75 kDynes) contusion via computer-controlled delivery. All SCI mice received fluid supplements (Lactated Ringer's solution, 1 mL; Hospira, Inc., Lake Forest, IL), antibiotics (Baytril, Norbrook Laboratories Limited, Newry, Northern Ireland; 10 mg/kg), and analgesics (buprenorphine, 0.05 mg/kg) subcutaneously for the first week (twice per day) following surgery. Twice daily bladder expressions continued for the duration of the study. Locomotor recovery was assessed using the Basso Mouse Scale[21] open field test at 1 d and weekly after injury.

Eight- to ten-week old female rats weighing 180–200 g were anesthetized (ketamine/xylazine, 45 mg/5 mg/kg intraperitoneally) before receiving a moderate T8 contusive spinal cord injury (200 kDynes) using the Infinite Horizon impactor device (Precision Systems and Instrumentation, Lexington, KY) for rats. Lactated Ringer's solution (3 mL), and the same doses of Baytril and buprenorphine as described above were administered subcutaneously immediately post-surgery and then twice a day for 7 d. Twice-daily bladder expressions were performed until end of the study. All procedures were in accordance with University of Miami Institutional Animal Care and Use Committee and National Institutes of Health guidelines.

Histology

Mice or rats were perfused transcardially with cold phosphate-buffered saline (PBS) followed by 4% paraformaldehyde. Brains and spinal cords were harvested, post-fixed for 2 h and placed in 10%, 20%, 30% sucrose gradient overnight. An 8-mm mouse or 12-mm rat spinal segment centered at the injury site was embedded in Optimal Cutting Temperature compound compound (Tissue-Tek, Sakura Finetek USA, Inc., Torrance, CA) and sectioned on a cryostat. Sagittal or horizontal sections were cut serially at 10 μm and immunostained in PBS-0.3% TritonX-100 for mouse fibronectin (Millipore, Billerica, MA; AB2033, 1:500) or rat fibronectin (Millipore AB1954, 1:500), integrin $\alpha5\beta1$ (Millipore MAB1984, 1:250), platelet-derived growth factor β (PDGFR-β; Abcam, Cambridge, MA; AB32570, 1:200), CD11b (Invitrogen, Grand Island, NY; RM2800, 1:500), glial fibrillary acidic protein (GFAP; Invitrogen 130300, 1:2000 or Abcam ab4674, 1:500), NeuN (Millipore MAB377, 1:300), Olig2 (Millipore AB9610, 1:250), RFP (red fluorescent protein; Rockland, Limerick, PA; 600-401-379S, 1:2000) and green fluorescent protein (GFP; Abcam, Cambridge, MA; ab13970, 1:1,000). Primary antibody incubation was followed by appropriate Alexa Fluor secondary antibodies (Invitrogen, 1:500). Sections were mounted in Vectashield containing 4′,6-diamidino-2-phenylindole (DAPI; Vector Laboratories, Burlingame, CA), and images were collected with a Nikon (Melville, NY) Eclipse Ti fluorescent microscope or an Olympus (Pittsburgh, PA) FluoView 1000 confocal microscope.

Western blot

Mice were anesthetized (see above) and perfused transcardially with cold PBS. A 4-mm spinal segment centered at the injury site was dissected and meninges removed. Spinal cord tissues were then chopped into 100-μm slices using a McIlwain Tissue Chopper (Stoelting Co., Redding, CH) and lysed using a deoxycholate (DOC) extraction protocol as previously described.[22] Chopped tissue in freshly prepared 2% DOC lysis buffer (2% DOC, 20mM Tris.Cl, 2mM EDTA, 2mM iodoacetic acid, 2mM N-ethylmaleimide, 2mM PMSF) was passed through a 25G needle and centrifuged (4°C, 15,000g) to obtain DOC-soluble (supernatant) and DOC-insoluble (pellet) components. The DOC-insoluble pellet was solubilized in freshly prepared 1% SDS lysis buffer (1% SDS, 20mM Tris.Cl, 2mM EDTA, 2mM iodoacetic acid, 2mM N-ethylmaleimide, 2mM PMSF) and centrifuged (room temperature, 15,000 g) to obtain supernatant that contained DOC-insoluble ECM. Protein concentration was measured using bicinchoninic acid assay (Thermo Scientific, Waltham, MA). Protein sample from individual animals (mixed in β-mercaptoethanol) were separated on a 4–15% Criterion TGX precast gel (Bio-rad, Hercules, CA) and transferred onto a polyvinylidene difluoride (PVDF) membrane that was blocked in 5% milk (in Tris-Buffered Saline and Tween; Sigma-Aldrich, St. Louis, MO) TBS-T and incubated in rabbit anti-fibronectin antibody (Millipore AB2033, 1:2000) overnight at 4°C.

The next day, membranes were washed and incubated in appropriate HRP-conjugated secondary antibodies (Jackson ImmunoResearch, West Grove, PA; 1:50,000) and detected using chemiluminescent substrate (SuperSignal West Pico Thermo Scientific, Waltham, MA) and exposed to film. To control for loading variations, transferred PVDF membranes were incubated in 0.1% Coomassie blue R250 in 50% methanol/water for 30 min and de-stained in acetic acid/ethanol/water (1:5:4) for 20 min as previously described.[23] Band densities were quantified via ImageJ. Destained membrane was dried completely overnight and scanned. Each complete lane was then selected and band densities quantified using ImageJ 1.47v. Densities of fibronectin bands were normalized to densities of Coomassie blue (Supplementary Fig. 1; see online supplementary material at www.liebertpub.com).

qRT-PCR

Mice were anesthetized (see above) and perfused transcardially with cold diethylpyrocarbonate PBS. A 4-mm spinal segment centered at the injury site was dissected and homogenized and total ribonucleic acid (RNA) extracted using Qiagen RNeasy Plus Micro Kit. Total RNA was treated with DNAase (AMPD1; Sigma-Aldrich, St. Louis, MO) and complementary deoxyribonucleic acid (cDNA) synthesized using the Advantage RT-PCR Kit (ClonTech, Mountain View, CA). Quantitative polymerase chain reaction (qPCR) was performed using SYBR Green PCR Master Mix (Applied Biosystems, Carlsbad, CA) and the Corbett Research RG 3000 thermal cycler (Qiagen, Valencia, CA). A standard curve was

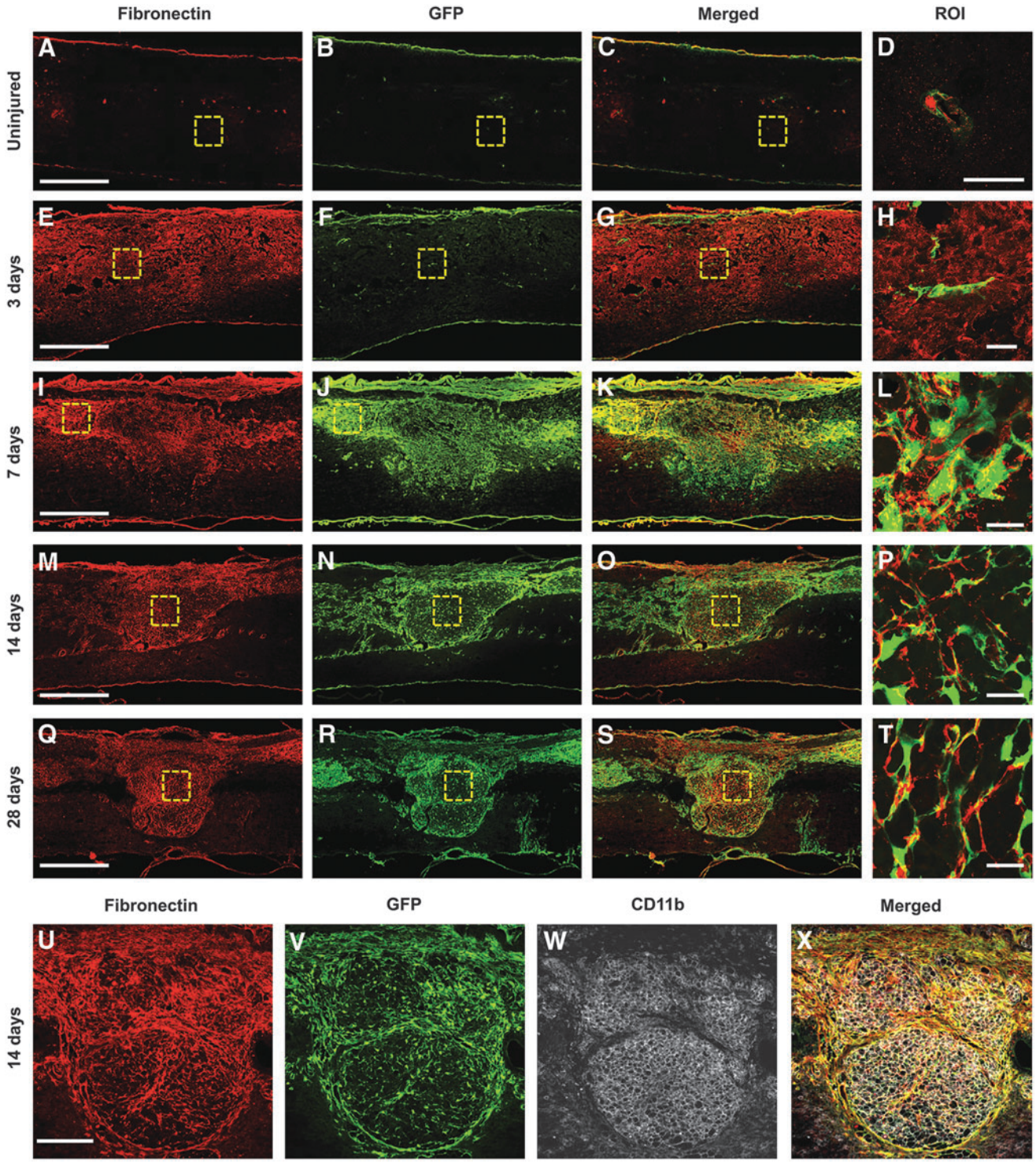

FIG. 1. Fibrotic scar formation after contusive spinal cord injury. In the uninjured spinal cord **(A-D)**, fibronectin (red) expression and fibroblasts (green) are found only around blood vessels **(D)** and in the dura. At 3 d after injury **(E-H)**, there is diffuse fibronectin expression throughout the injury site **(E)** while fibroblasts are not present in significant numbers **(F)**. At 7 d **(I-L)**, when fibroblasts densely populate the injury site **(J)**, the area of fibronectin expression closely matches that of fibroblasts **(K)** and appears more punctate **(L)**. At 14 d **(M-P, U-X)**, when the fibrotic scar has matured, it is characterized by a dense population of mostly fibroblasts and $CD11b^+$ leukocytes **(W)** and a fibronectin expression network that closely follows the distribution of fibroblasts throughout the injury site. This pattern continues at 28 d **(Q-T)**. $n = 5$ per group. Scale bar in A, E, I, M, Q = 500 μm; in D, H, L, P, T = 50 μm; in U = 200 μm.

generated for each primer pair using serial dilutions of liver cDNA to optimize PCR conditions for each primer set. Expression level of each gene was calculated using the ΔΔCt method and normalized to glyceraldehyde 3-phosphate dehydrogenase. Each sample was tested in triplicates. The primer sequences were: itga5 (forward: GGACCAAGACGGCTACAATGATGT, reverse: ACCTGGGAA GGTTTAGTGCTCAGT), itgb1 (forward: TTCAGACTTCCGCA TTGGCTTTGG, reverse: TGGGCTGGTGCAGTTTTGTTCAC), itgav (forward: GGGCCTATTGTTCAGCACAT, reverse: GATTC CACAGCCCAAAGTGT). The primer set for itgb3 was purchased from Qiagen (QT00128849, QuantiTect Primer Assay).

Quantification

Quantifications of immunohistochemical images were performed by unbiased observers. To quantify the number of $\alpha5\beta1^+$ cells that are also $CD11b^+$ or GFP^+, co-localized cells were counted in three randomly selected 100 μm × 100 μm squares in the $GFAP^-$ region (fibrotic scar). Only $DAPI^+$ cells were counted. Co-localization was verified using Olympus FV10-ASW 3.0 viewer software to examine each of the ten one-micron Z-stack slices. For each animal, sections including the injury epicenter and two adjacent sagittal sections (spaced 100 μm apart) were quantified, and

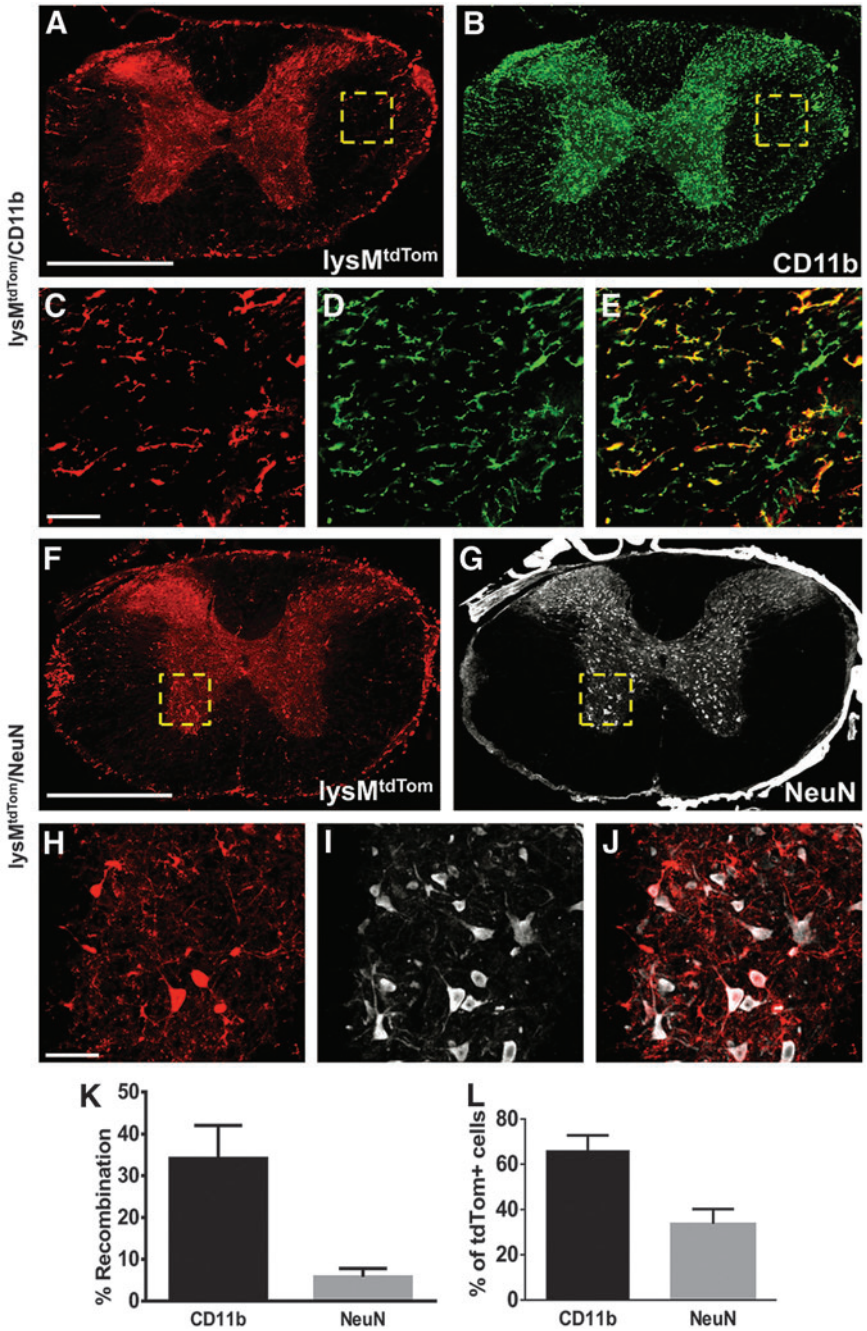

FIG. 2. Recombination rate in uninjured spinal cord of lysM-Cre mice. lysM-Cre/Rosa26-tdTomato mice demonstrate that approximately 34% of all microglia (CD11b) have undergone recombination (tdTomato) **(A-E, K)**. A small percent of neurons (NeuN, 6%) also were labeled with tdTomato **(F-J, K)**. Of all the cells that underwent recombination (tdTomato), approximately 66% were microglia and 33% were neurons **(L)**. $n = 3$. Scale bar in **A,** F = 500 μm; in **C,** H = 50 μm. Error bars are standard error of the mean.

the counts from each section were averaged. A total of 150–300 cells per animal were counted.

Quantification of the lysM^{tdTom} cells in uninjured tissue were based on co-localization of the tdTomato reporter signal (enhanced using RFP antibody) with the following cell markers: CD11b, NeuN, GFAP and Olig2. Only DAPI$^+$ cells were counted. A total of 150–300 cells per animal were counted across at least three adjacent coronal sections (spaced 100 μm apart) of the thoracic spinal cord.

Results

Fibronectin matrix and fibroblasts have similar spatiotemporal distribution after SCI

Since the fibrotic scar is best characterized by regions of high fibronectin expression and fibroblast infiltration, we sought to determine the spatiotemporal relationship between fibronectin and fibroblasts after SCI. We utilized collagen1α1-GFP transgenic mice, which we have previously described as labeling perivascular fibroblasts in the spinal cord.[15] In the uninjured spinal cord, fibroblasts and fibronectin were found only around blood vessels and in the meninges (Fig. 1A-D). At 3 d after injury, while fibronectin expression was increased, compared with uninjured spinal cord, its staining pattern was very diffuse throughout the injury site, suggesting that fibronectin had not yet formed into a fibrillar matrix. Importantly, fibroblasts were not present in significant number, suggesting that fibronectin was most likely from blood plasma and that the presence of fibronectin at this acute time point is not a reliable indicator of fibrotic scar formation (Fig. 1E-H). However, at 7 d, there were a large number of fibroblasts present at the injury site and their distribution pattern closely matched that of fibronectin expression (Fig. 1I-L). In addition, while fibronectin expression appeared very diffuse at 3 d after injury, it became much more condensed and fibrillar by 7 d, indicating that fibronectin was starting to form into a matrix. At 14 d, when the fibrotic scar has started to mature, fibronectin expression became much more organized into a fibrillar network that closely resembled the fibroblast distribution pattern (Fig. 1M-P, U-X). At this time, CD11b$^+$ leukocytes also filled the fibrotic scar and were intimately associated with fibroblasts. This phenotype continued at 28 d (Fig. 1Q-T). Hence, these results demonstrate a matching distribution pattern between the fibronectin matrix and infiltration of perivascular fibroblasts at the injury site.

Fibroblasts are likely the primary source of fibronectin in the fibrotic scar

Although the expression pattern of fibronectin suggests that fibroblasts are the source of fibronectin, it is possible that activated macrophages/microglia could also contribute. Thus, we sought to determine whether macrophages/microglia are a source of

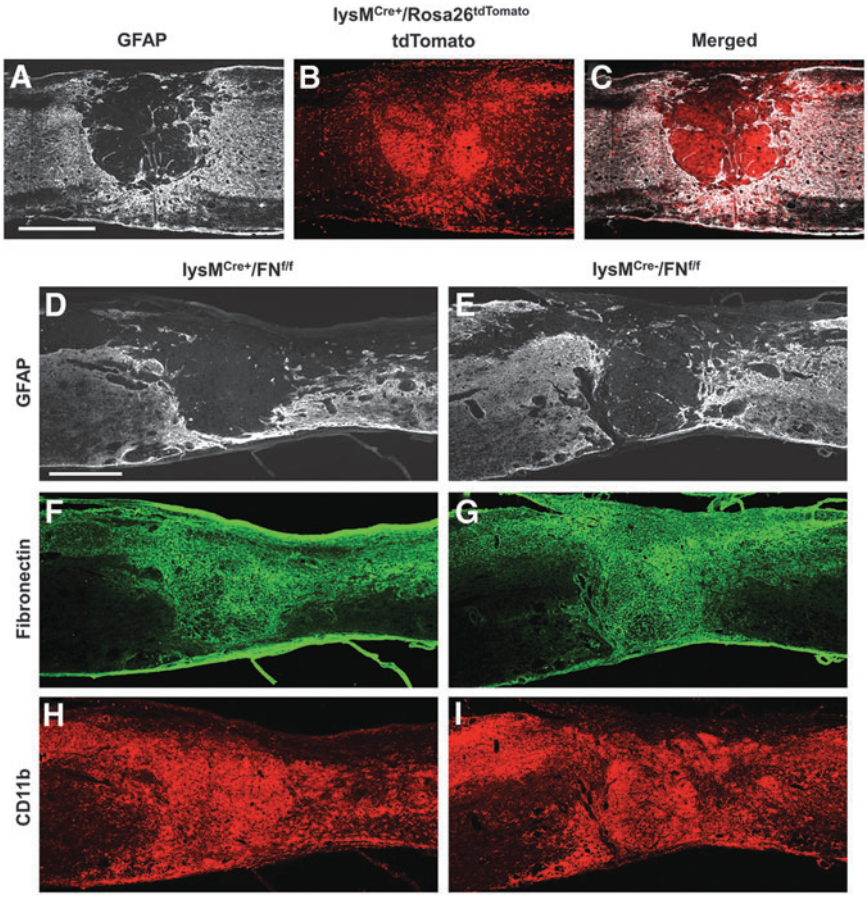

FIG. 3. Activated macrophages/microglia are not a major source of fibronectin after spinal cord injury. Breeding lysM-Cre mice to Rosa26-tdTomato reporter mice demonstrates the distribution of myeloid cells at the injury site that have undergone recombination (**A-C**, 14 d after injury, $n=3$). Genetic deletion of fibronectin (FN) in myeloid cells (lysM-Cre bred to floxed FN mouse; **D, F, H**; $n=5$) does not show visible differences in CD11b$^+$ leukocyte infiltration and FN expression at the injury site, compared with Cre$^-$ controls (**E, G, I**; 14 d after injury; $n=5$). Scale bar in **A,** D = 500 μm.

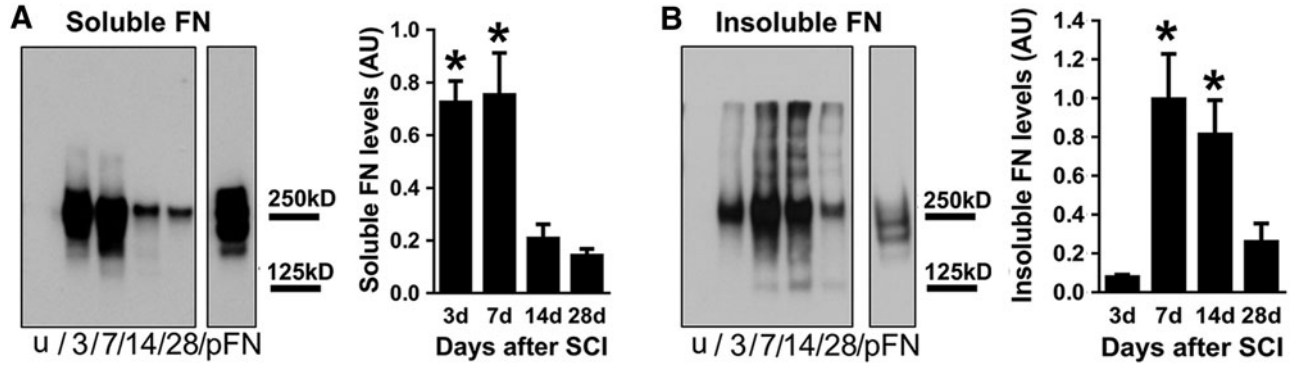

FIG. 4. Fibronectin matrix assembly after spinal cord injury (SCI). Soluble fibronectin is significantly increased at 3 and 7 d after SCI and then decreases over time, albeit still at higher levels than uninjured spinal cord (**A**; $n = 5$ per group). Insoluble fibronectin (indicated by multiple bands above the 250 kD monomer band) is highest at 7 and 14 d after injury (**B**, $n = 5$ per group). Purified plasma fibronectin (pFN) was used as a positive control and loaded in equal amounts in both blots. Note the absence of > 250 kD bands in the soluble fraction **(A)** even after a longer film exposure time (as indicated by darker pFN band in **A** compared with **B**). The entire blot is shown in Supplementary Figure 1. $*p < 0.05$ compared with 14 d, 28 d in **A**; 3 d, 28 d in **B** using one way analysis of variance with Tukey's post-test. Error bars are standard error of the mean.

fibronectin by deleting fibronectin in these cells. The lysM-Cre knock-in mouse line expresses Cre recombinase in myeloid cells, including most macrophages and granulocytes.[24] While this mouse line has been well-characterized in terms of recombination in peripheral organs, no one has reported its recombination efficiency in mouse spinal cord. Thus, we used lysM^{tdTom} mice (lysM-Cre mice crossed with Rosa26-tdTomato reporter mice) to determine the recombination efficiency of lysM-Cre in the uninjured spinal cord. We performed immunohistochemistry to co-label tdTomato with microglia (CD11b$^+$), neurons (NeuN$^+$), astrocytes (GFAP$^+$), and oligodendrocyte lineage cells (Olig2$^+$). In the uninjured spinal cord, tdTomato labeled approximately 34% of all CD11b$^+$ microglia (Fig. 2A-E, K). This is in accordance with a recent report showing about 40% lysM-Cre efficiency in microglia isolated from uninjured spinal cord using flow cytometry.[25] This recombination efficiency for microglia is relatively low, compared with the 80–90% recombination efficiency reported for mature macrophages.[24,26] Surprisingly, we also observed around 6% of neurons that underwent recombination (Fig. 2F-J, K). No tdTomato expression was observed in GFAP$^+$ or Oligo2$^+$ cells (data not shown). Of all the tdTomato$^+$ cells, approximately 66% were microglia and the rest were neurons (Fig. 2L).

Next, we injured lysM^{tdTom} mice to determine the expression pattern of lysM-Cre recombinase after SCI. We found that the fibrotic scar (GFAP$^-$ area) was filled with tdTomato$^+$ cells (Fig. 3A-C), suggesting that the recombination efficiency is very high in myeloid cells that occupy the fibrotic scar. We then performed SCI on lysM^{Cre+}/FN$^{fl/fl}$ mice (lysM-Cre mice crossed with floxed fibronectin mice). We found that while CD11b$^+$ cells were densely concentrated in the fibrotic scar (Fig. 3H, I), there were no visible differences in fibronectin expression level, compared with Cre$^-$ controls (Fig. 3F, G). Our results rule out macrophages/microglia as a major source of fibronectin and suggest that fibroblasts are most likely the primary source of fibronectin in the fibrotic scar.

Fibronectin matrix assembly after SCI

While the fibrillar organization of fibronectin at 7 d and beyond suggested its assembly into a matrix, we confirmed our observation using a biochemical approach by comparing the DOC-soluble and insoluble fractions of the injury site using western blot analysis. Fibronectin that has not assembled into a matrix is DOC-soluble, while matrix fibronectin is DOC-insoluble. In the uninjured spinal cord, both soluble and insoluble fibronectin were below detectable levels (Fig. 4A, B; Supplementary Fig. 1), consistent with our immunohistochemistry results above (Fig. 1A). There was a large increase in soluble fibronectin at 3 d after injury, peaking at 7 d and then dramatically decreasing at 14 and 28 d (Fig. 4A; Supplementary Fig. 1). Insoluble fibronectin is indicated by multiple bands above the expected 250 kD monomer band. These multiple bands are present only in the insoluble fraction and contain fibronectin polymers that may be still in an interconnected matrix form. Insoluble fibronectin showed dramatic increases at 7 and 14 d after injury and decreased by 28 d (Fig. 4B; Supplementary Fig. 1). This suggests that soluble fibronectin expressed acutely after injury (3 d) is replaced by insoluble matrix fibronectin at later time points and that there is a decrease in overall fibronectin expression by 28 d after injury.

In addition to the multiple bands above 250 kD, there are 125 kD lower bands that are also only specific to the insoluble fraction from 7 through 28 d (Fig. 4B). This temporal distribution coincides with fibronectin matrix formation revealed by immunohistochemistry (Fig. 1A, 1E, 1I, 1M, and 1Q), suggesting that the 125 kD bands may be proteolytic products of the fibronectin matrix, which is a result of ECM dynamics after SCI. Taken together, our data indicates that while fibronectin is highly expressed as early as 3 d after injury, its assembly into a matrix occurs at around 7 d when there is a large accumulation of fibroblasts and macrophages/microglia at the injury site.

Fibroblasts and macrophages/microglia express α5β1 fibronectin receptor

To investigate the mechanism of fibronectin matrix assembly, we studied the expression of $\alpha5\beta1$ and $\alpha V\beta3$ integrin receptors, which are the two major fibronectin receptors that have been described to participate in fibronectin assembly in vivo.[27–29] Using qRT-PCR, we found that in the uninjured spinal cord, $\alpha5$ subunit had the lowest expression, compared with the other subunits (Fig. 5A), confirming barely detectable levels of $\alpha5\beta1$ immunoreactivity in uninjured spinal cord tissue sections (data not shown). However, after SCI, there was a 30- to 40-fold increase in $\alpha5$ gene expression at 7 and 28 d after injury (Fig. 5B). There also was a significant increase in $\beta1$ expression, while αV and $\beta3$ subunits showed an increasing trend

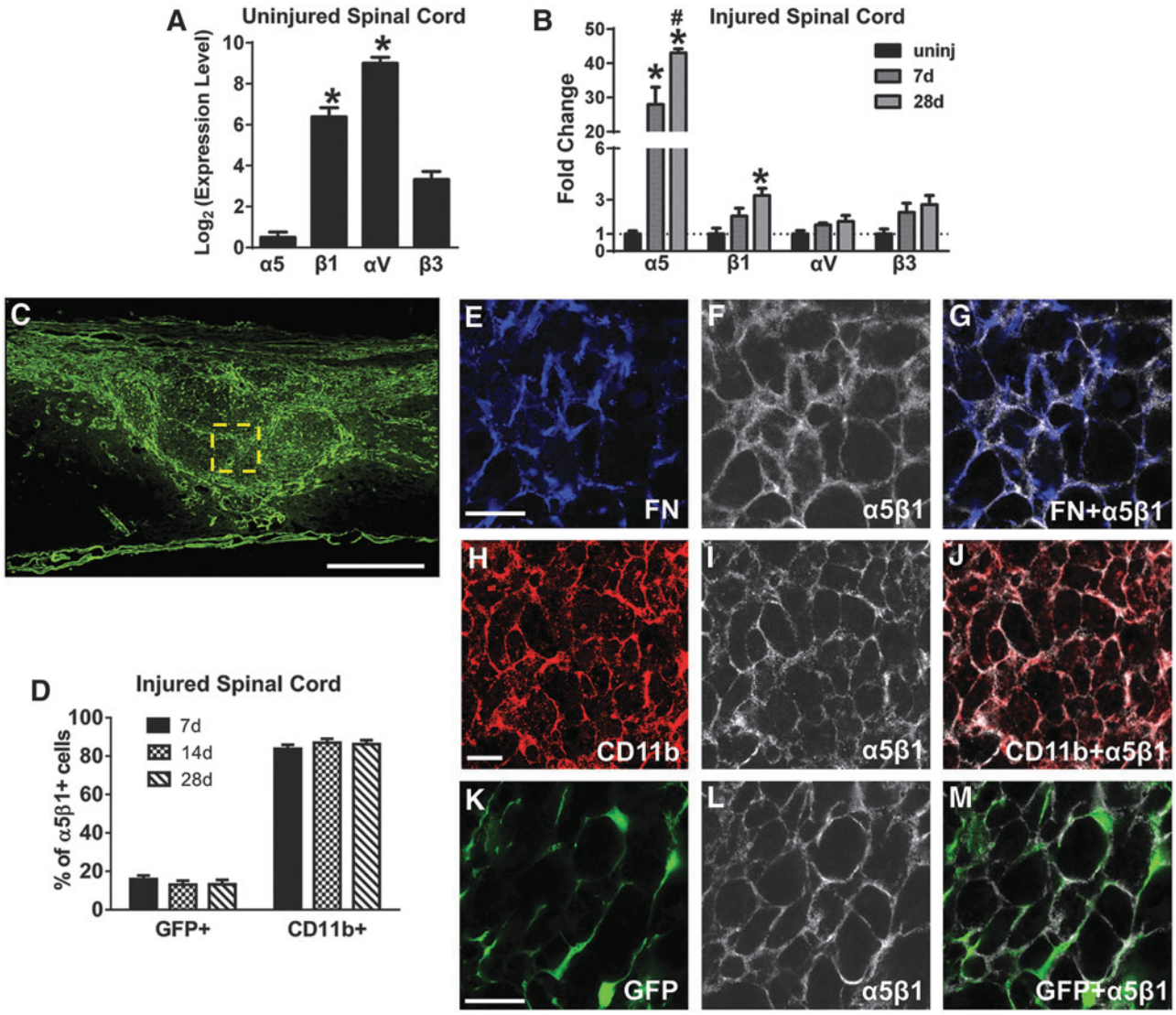

FIG. 5. Integrin receptor $\alpha5\beta1$ is expressed by macrophages/microglia and fibroblasts after spinal cord injury (SCI). In the uninjured spinal cord, αV and $\beta1$ integrin subunit messenger RNA (mRNA) levels are higher than $\alpha5$ and $\beta3$ (**A**, $n=3$ per group). After SCI, both $\alpha5$ and $\beta1$ mRNA are significantly increased, while αV and $\beta3$ mRNA levels are not significantly altered (**B**, $n=3$ per group). Within the fibrotic scar at 14 d after injury **(C)**, fibronectin is present mostly in regions of $\alpha5\beta1$ expression **(E-G)**, which is present on $CD11b^+$ macrophages/microglia (**H-J, D**; $n=3$ per group) and fibroblasts (**K-M, D**; $n=3$ per group). C, E, H, K are from different animals. Scale bar in C = 500 μm; in E, H, K = 50 μm. A: $*p<0.05$ compared with $\alpha5$, $\beta3$ using one way analysis of variance (ANOVA) with Tukey's post-test. B: $*p<0.05$ compared with uninjured (uninj), $\#p<0.05$ compared with 7 d, two-way ANOVA with Bonferonni post-test. Error bars are standard error of the mean.

that did not reach statistical significance (Fig. 5B). Therefore, $\alpha5$ and $\beta1$ expression showed the largest changes after injury and virtually all fibronectin co-localized with $\alpha5\beta1$ (Fig. 5E-G), suggesting that the $\alpha5\beta1$ integrin receptor may be the primary fibronectin receptor after SCI. It should be noted, however, that not all $\alpha5\beta1$ receptor co-localized with fibronectin, suggesting that this receptor may have functions other than fibronectin assembly in the fibrotic scar.

To determine the cell types that express $\alpha5\beta1$, we performed immunohistochemistry to co-label $\alpha5\beta1$ with different cellular markers. Since the fibrotic scar is comprised mainly of fibroblasts and immune cells, we focused on $Col1\alpha1\text{-}GFP^+$ fibroblasts and $CD11b^+$ cells. Inside the fibrotic scar, approximately 80% and 20% of $\alpha5\beta1^+$ cells were $CD11b^+$ and $Col1\alpha1\text{-}GFP^+$, respectively (Fig. 5H-M, 5D). Since most $CD11b^+$ cells are macrophages/microglia at this time after SCI,[30] our data suggests that activated macrophages/microglia may play a role in fibronectin matrix assembly in the fibrotic scar.

Fibrotic scar is present in injured rat spinal cord

To determine whether the fibrotic scar is present in a more clinically relevant animal model, we performed contusive SCI in rats, of which the pathological features are considered more similar to human SCI.[16,31–33] At 56 d after injury, we assessed the injury site for fibronectin and PDGFR-β expression as markers for the fibrotic scar, because we demonstrated in our mouse model that fibronectin is abundantly present in the fibrotic scar (Fig. 1) and virtually all $Col1\alpha1\text{-}GFP^+$ fibroblasts comprising the fibrotic scar express PDGFR-β.[15] Using immunohistochemistry, we detected intense immunoreactivity for fibronectin and PDGFR-β along the peripheral

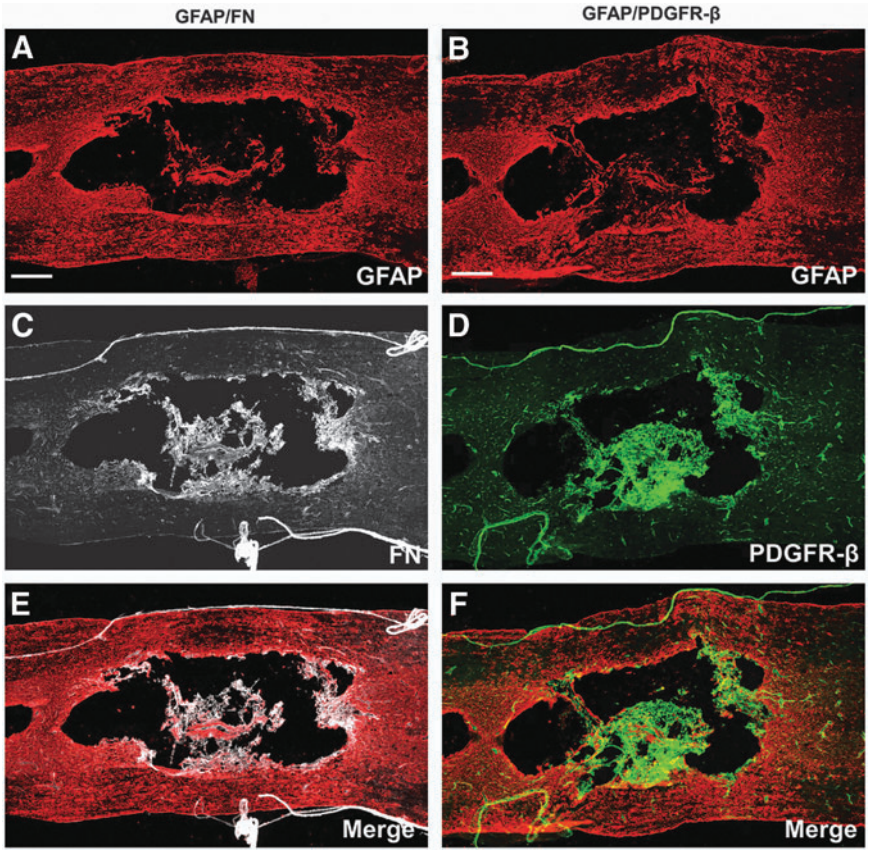

FIG. 6. Presence of fibrotic scar in rat injury site. Images **(A-F)** are taken from horizontal sections of rat spinal cord 56 d after a moderate contusion ($n = 4$). GFAP represents the astroglial scar and is expressed throughout the entire injury site **(A, B)** after spinal cord injury. Expression of fibronectin (FN) and PDGFR-β (a marker for fibroblasts) is found on blood vessels, meninges, and lining the cavity (C-F). Scale bar in **A,** B = 500 μm.

rim of the cavities and outlining blood vessels in the surrounding spared tissue (Fig. 6) in rats. However, instead of taking up all GFAP$^-$ regions as in mice, the fibrotic scar in rats occupied a relatively smaller area at the injury site due to the distinct cavitation that has occurred in the fibrotic regions (Fig. 6C, D). Note that the rat spinal cords are presented in horizontal sections as opposed to sagittal sections of mouse spinal cords shown above, so the morphologies of the injury site look different due to different observation planes.

Similar to what is seen in mice, fibronectin and PDGFR-β had similar expression patterns at the rat injury site (Fig. 6C, D). However, in sharp contrast to the non-overlapping staining pattern between fibronectin and GFAP in mice (Fig. 3D-G), there was more overlap between GFAP$^+$ regions with fibronecin$^+$ and PDGFR-β^+ regions in rats (Fig. 6E, F). Taken together, our findings indicate that the fibrotic scar is present in injured rat spinal cord, and suggest that it may also be present in injured human spinal cord.

Discussion

We sought to determine the mechanism of fibrotic scar formation after SCI by focusing on fibronectin matrix assembly. Our data indicate that while fibronectin is present at the injury site as early as 3 d after SCI, it starts to form a matrix around 7 d. This coincides with the time of peak fibroblast[15] and macrophage/microglia[34] infiltration, both of which express the prototypical fibronectin receptor integrin $\alpha 5\beta 1$. We determined that activated macrophages/microglia are not a source of fibronectin by deleting fibronectin in myeloid cells, suggesting that fibroblasts are likely the primary source of fibronectin after SCI. Finally, we demonstrate the presence of fibrotic scar markers such as fibronectin and PDGFR-β at the rat spinal cord injury site, suggesting that fibrotic scarring after SCI may be present across species.

Much of our knowledge of fibronectin comes from studies of cutaneous wound healing and peripheral organ fibrosis, in which fibronectin is suggested as a scaffolding protein that regulates ECM deposition and support cell adhesion, migration and survival. For example, in later phases of skin wound healing, the fibronectin matrix regulates deposition of other ECM molecules such as fibrinogen, collagen, laminin, chondroitin sulfate proteoglycan (CSPG), and tenascin-C.[35,36] Fibronectin also is found to attract fibroblasts in glomerular fibrosis,[37] and support migration and survival of both circulating monocytes and microglia.[38–40]

In central nervous system (CNS) injury, plasma fibronectin frequently is used as a component in biomaterial-based and/or cell-based grafts to facilitate cell migration, adhesion, and survival, and promote axon regeneration.[41–44] Moreover, plasma fibronectin has been shown to have a neuroprotective role in brain injury[45] and ischemia.[46] Although fibronectin is the most commonly used marker of the fibrotic scar, virtually nothing is known about its role in the pathophysiology of SCI. Since fibronectin itself is neuroprotective and growth permissive for axons, why is the fibronectin-abundant fibrotic scar so inhibitory to axon regeneration? A possible explanation would be that inhibitory molecules bind to the fibronectin matrix after SCI and result in an inhibitory environment

in the fibrotic scar. This is supported by reports that the fibronectin matrix is closely associated with inhibitory proteins, such as NG2 proteoglycan and tenascin-C, in astrocytes/fibroblasts co-culture[4] and in SCI lesion epicenter.[47,48] Further, fibronectin molecule has binding sites for the glycosaminoglycan chains of CSPGs and it has been demonstrated that CSPGs interact with fibronectin in vitro using various binding assays.[49–51] It is important to note that in order for these interactions to occur, fibronectin typically needs to form into a matrix, which we have demonstrated in this study. Therefore, understanding how the fibronectin matrix is assembled after SCI may allow us to target multiple inhibitory molecules in the fibrotic scar in order to promote axon regeneration.

Based on the functions of fibronectin described above, we hypothesize that fibronectin present at 3 d after SCI is most likely plasma fibronectin from blood, which is involved in formation of the provisional clot to stop bleeding. This provisional matrix provides a substrate for fibroblast and macrophage/microglia migration, which reaches a peak by 7 d. We propose that fibroblasts express cellular fibronectin that is assembled into a matrix mostly by macrophages/activated microglia. This peak in cellular migration also corresponds to peak soluble and insoluble fibronectin expression and regulation, as indicated by matrix assembly and degradation. At 14 d after injury, matrix fibronectin remains abundant while the level of soluble fibronectin significantly decreases, perhaps due to a combination of re-establishment of the blood–spinal cord barrier[52,53] and degradation of plasma fibronectin by infiltrating cells. By 28 d after injury, matrix fibronectin levels also decline significantly and this could be due to a decrease in the number of fibroblasts at this time.[15] However, more functional studies are needed to support this working model.

For example, since it remains possible that fibroblasts simply assemble the fibronectin that is expressed by another cell type, future studies will need to delete fibronectin specifically in fibroblasts to address this issue. In addition, this loss-of-function study also will address what role, if any, fibronectin play in fibrotic scar formation. In addition, while the expression of $\alpha5\beta1$ integrin mostly on macrophages/microglia suggests that these cells might play a role in assembly of fibronectin into a matrix, a genetic deletion of the receptor specifically in these cells is necessary to reach a more firm conclusion.

Rat contusive SCI model is generally considered more relevant to human pathology than that of mouse. Unlike mouse contusive SCI, in which a profound fibrotic scar forms that fills up the entire lesion epicenter, rat injury site undergoes cavity formation that resembles human SCI patients.[31,54] Because of this prominent cavitation, whether fibrotic scarring plays a role after human contusive SCI has received less attention. In our study using a rat model of contusive SCI, we clearly show that fibronectin$^+$ ECM and PDGFR-β^+ fibroblasts are present at the injury site, indicating that fibrotic scarring also occurs after rat SCI. However, in contrast to the distinct non-overlapping regions of fibronectin/PDGFR-β and GFAP expression in mice, there was some overlap of these regions in rats, suggesting that astrocytes may also play a role in fibrotic scarring rats and that there may be some differences in fibrotic mechanisms between the two species.

Moreover, given the observation that the fibrotic scar is always present along the cavity wall in rats, we could infer that a diminished fibrotic scarring may be the cause of the significant cavitation after rat SCI. This is in sharp contrast to the dense fibrotic scar in mice where cavitation does not happen. Whether this is the result of differences in the immune response between rats and mice or due to more direct differences in fibroblasts between the two species remains to be investigated.

In summary, our data indicates that fibronectin forms a matrix after SCI and that it is most likely expressed by fibroblasts at the injury site. In addition, we demonstrate that SCI in rats also leads to fibrotic scar formation (albeit to a lesser extent than in mice), suggesting that it also may be relevant to human SCI pathology.

Acknowledgments

We thank Dr. Takao Sakai for the floxed fibronectin mice, Dr. David Brenner and Dr. Tatiana Kisseleva for the Col1α1-GFP transgenic mice, and Dr. Fan Wang for the Rosa26-tdTomato reporter mice. We thank Dr. Melissa Carballosa-Gautam at the Miami Project Imaging Core for assistance with microscopy. We thank Dr. Kirill Lyapichev and Yadira Salgueiro for technical assistance. This study was funded by NINDS R01NS081040, R21NS082835, U.S. Army W81XWH131007715, The Miami Project to Cure Paralysis, and the Buoniconti Fund.

Author Disclosure Statement

No competing financial interests exist.

References

1. Cregg, J.M., Depaul, M.A., Filous, A.R., Lang, B.T., Tran, A. and Silver, J. (2014). Functional regeneration beyond the glial scar. Exp. Neurol. 253C, 197–207.
2. Burda, J.E. and Sofroniew, M.V. (2014). Reactive gliosis and the multicellular response to CNS damage and disease. Neuron 81, 229–248.
3. Shearer, M.C. and Fawcett, J.W. (2001). The astrocyte/meningeal cell interface–a barrier to successful nerve regeneration? Cell Tissue Res. 305, 267–273.
4. Kimura-Kuroda, J., Teng, X., Komuta, Y., Yoshioka, N., Sango, K., Kawamura, K., Raisman, G., and Kawano, H. (2010). An in vitro model of the inhibition of axon growth in the lesion scar formed after central nervous system injury. Mol. Cell. Neurosci. 43, 177–187.
5. Wanner, I.B., Deik, A., Torres, M., Rosendahl, A., Neary, J.T., Lemmon, V.P., and Bixby, J.L. (2008). A new in vitro model of the glial scar inhibits axon growth. Glia 56, 1691–1709.
6. Goritz, C., Dias, D.O., Tomilin, N., Barbacid, M., Shupliakov, O., and Frisen, J. (2011). A pericyte origin of spinal cord scar tissue. Science 333, 238–242.
7. Herrmann, J.E., Shah, R.R., Chan, A.F., and Zheng, B. (2010). EphA4 deficient mice maintain astroglial-fibrotic scar formation after spinal cord injury. Exp. Neurol. 223, 582–598.
8. Bundesen, L.Q., Scheel, T.A., Bregman, B.S., and Kromer, L.F. (2003). Ephrin-B2 and EphB2 regulation of astrocyte-meningeal fibroblast interactions in response to spinal cord lesions in adult rats. J. Neurosci. 23, 7789–7800.
9. Stoffels, J.M., de Jonge, J.C., Stancic, M., Nomden, A., van Strien, M.E., Ma, D., Siskova, Z., Maier, O., Ffrench-Constant, C., Franklin, R.J., Hoekstra, D., Zhao, C., and Baron, W. (2013). Fibronectin aggregation in multiple sclerosis lesions impairs remyelination. Brain 136, 116–131.
10. Gratchev, A., Guillot, P., Hakiy, N., Politz, O., Orfanos, C.E., Schledzewski, K., and Goerdt, S. (2001). Alternatively activated macrophages differentially express fibronectin and its splice variants and the extracellular matrix protein betaIG-H3. Scand. J. Immunol. 53, 386–392.
11. Singh, P., Carraher, C., and Schwarzbauer, J.E. (2010). Assembly of fibronectin extracellular matrix. Annu. Rev. Cell Dev. Biol. 26, 397–419.
12. Danen, E.H. and Yamada, K.M. (2001). Fibronectin, integrins, and growth control. J. Cell Physiol. 189, 1–13.
13. Schwarzbauer, J.E. and DeSimone, D.W. (2011). Fibronectins, their fibrillogenesis, and in vivo functions. Cold Spring Harb. Perspect. Biol. 3.
14. To, W.S. and Midwood, K.S. (2011). Plasma and cellular fibronectin: distinct and independent functions during tissue repair. Fibrogenesis Tissue Repair 4, 21.
15. Soderblom, C., Luo, X., Blumenthal, E., Bray, E., Lyapichev, K., Ramos, J., Krishnan, V., Lai-Hsu, C., Park, K.K., Tsoulfas, P., and Lee, J.K. (2013). Perivascular fibroblasts form the fibrotic scar after contusive spinal cord injury. J. Neurosci. 33, 13882–13887.

16. Norenberg, M.D., Smith, J., and Marcillo, A. (2004). The pathology of human spinal cord injury: defining the problems. J. Neurotrauma 21, 429–440.
17. Guest, J.D., Hiester, E.D., and Bunge, R.P. (2005). Demyelination and Schwann cell responses adjacent to injury epicenter cavities following chronic human spinal cord injury. Exp. Neurol. 192, 384–393.
18. Yata, Y., Scanga, A., Gillan, A., Yang, L., Reif, S., Breindl, M., Brenner, D.A., and Rippe, R.A. (2003). DNase I-hypersensitive sites enhance alpha1(I) collagen gene expression in hepatic stellate cells. Hepatology 37, 267–276.
19. Arenkiel, B.R., Hasegawa, H., Yi, J.J., Larsen, R.S., Wallace, M.L., Philpot, B.D., Wang, F., and Ehlers, M.D. (2011). Activity-induced remodeling of olfactory bulb microcircuits revealed by monosynaptic tracing. PLoS One 6, e29423.
20. Moriya, K., Bae, E., Honda, K., Sakai, K., Sakaguchi, T., Tsujimoto, I., Kamisoyama, H., Keene, D.R., Sasaki, T., and Sakai, T. (2011). A fibronectin-independent mechanism of collagen fibrillogenesis in adult liver remodeling. Gastroenterology 140, 1653–1663.
21. Basso, D.M., Fisher, L.C., Anderson, A.J., Jakeman, L.B., McTigue, D.M., and Popovich, P.G. (2006). Basso Mouse Scale for locomotion detects differences in recovery after spinal cord injury in five common mouse strains. J. Neurotrauma 23, 635–659.
22. Wierzbicka-Patynowski, I., Mao, Y., and Schwarzbauer, J.E. (2004). Analysis of fibronectin matrix assembly. Curr. Protoc. Cell Biol. Chapter 10, Unit 10 12.
23. Welinder, C. and Ekblad, L. (2011). Coomassie staining as loading control in Western blot analysis. J Proteome Res 10, 1416–1419.
24. Clausen, B.E., Burkhardt, C., Reith, W., Renkawitz, R., and Forster, I. (1999). Conditional gene targeting in macrophages and granulocytes using LysMcre mice. Transgenic Res. 8, 265–277.
25. Goldmann, T., Wieghofer, P., Muller, P.F., Wolf, Y., Varol, D., Yona, S., Brendecke, S.M., Kierdorf, K., Staszewski, O., Datta, M., Luedde, T., Heikenwalder, M., Jung, S., and Prinz, M. (2013). A new type of microglia gene targeting shows TAK1 to be pivotal in CNS autoimmune inflammation. Nat. Neurosci. 16, 1618–1626.
26. Abram, C.L., Roberge, G.L., Hu, Y., and Lowell, C.A. (2014). Comparative analysis of the efficiency and specificity of myeloid-Cre deleting strains using ROSA-EYFP reporter mice. J. Immunol. Methods 408, 89–100.
27. van der Flier, A., Badu-Nkansah, K., Whittaker, C.A., Crowley, D., Bronson, R.T., Lacy-Hulbert, A., and Hynes, R.O. (2010). Endothelial alpha5 and alphav integrins cooperate in remodeling of the vasculature during development. Development 137, 2439–2449.
28. Yang, J.T., Bader, B.L., Kreidberg, J.A., Ullman-Cullere, M., Trevithick, J.E., and Hynes, R.O. (1999). Overlapping and independent functions of fibronectin receptor integrins in early mesodermal development. Dev. Biol. 215, 264–277.
29. Takahashi, S., Leiss, M., Moser, M., Ohashi, T., Kitao, T., Heckmann, D., Pfeifer, A., Kessler, H., Takagi, J., Erickson, H.P., and Fassler, R. (2007). The RGD motif in fibronectin is essential for development but dispensable for fibril assembly. J. Cell Biol. 178, 167–178.
30. Kigerl, K.A., McGaughy, V.M., and Popovich, P.G. (2006). Comparative analysis of lesion development and intraspinal inflammation in four strains of mice following spinal contusion injury. J Comp. Neurol. 494, 578–594.
31. Byrnes, K.R., Fricke, S.T., and Faden, A.I. (2010). Neuropathological differences between rats and mice after spinal cord injury. J. Magn. Reson. Imaging 32, 836–846.
32. Sroga, J.M., Jones, T.B., Kigerl, K.A., McGaughy, V.M., and Popovich, P.G. (2003). Rats and mice exhibit distinct inflammatory reactions after spinal cord injury. J. Comp. Neurol. 462, 223–240.
33. Surey, S., Berry, M., Logan, A., Bicknell, R., and Ahmed, Z. (2014). Differential cavitation, angiogenesis and wound-healing responses in injured mouse and rat spinal cords. Neuroscience 275, 62–80.
34. Donnelly, D.J. and Popovich, P.G. (2008). Inflammation and its role in neuroprotection, axonal regeneration and functional recovery after spinal cord injury. Exp. Neurol. 209, 378–388.
35. Singer, A.J. and Clark, R.A. (1999). Cutaneous wound healing. N Engl. J. Med. 341, 738–746.
36. Rhett, J.M., Ghatnekar, G.S., Palatinus, J.A., O'Quinn, M., Yost, M.J., and Gourdie, R.G. (2008). Novel therapies for scar reduction and regenerative healing of skin wounds. Trends Biotechnol. 26, 173–180.
37. Gharaee-Kermani, M., Wiggins, R., Wolber, F., Goyal, M., and Phan, S.H. (1996). Fibronectin is the major fibroblast chemoattractant in rabbit anti-glomerular basement membrane disease. Am. J. Pathol. 148, 961–967.
38. Trial, J., Baughn, R.E., Wygant, J.N., McIntyre, B.W., Birdsall, H.H., Youker, K.A., Evans, A., Entman, M.L., and Rossen, R.D. (1999). Fibronectin fragments modulate monocyte VLA-5 expression and monocyte migration. J. Clin. Invest. 104, 419–430.
39. Nasu-Tada, K., Koizumi, S., and Inoue, K. (2005). Involvement of beta1 integrin in microglial chemotaxis and proliferation on fibronectin: different regulations by ADP through PKA. Glia 52, 98–107.
40. Abshire, M.Y., Thomas, K.S., Owen, K.A. and Bouton, A.H. (2011). Macrophage motility requires distinct alpha5beta1/FAK and alpha4-beta1/paxillin signaling events. J. Leukoc. Biol. 89, 251–257.
41. Geller, H.M. and Fawcett, J.W. (2002). Building a bridge: engineering spinal cord repair. Exp. Neurol. 174, 125–136.
42. King, V.R., Alovskaya, A., Wei, D.Y., Brown, R.A., and Priestley, J.V. (2010). The use of injectable forms of fibrin and fibronectin to support axonal ingrowth after spinal cord injury. Biomaterials 31, 4447–4456.
43. King, V.R., Hewazy, D., Alovskaya, A., Phillips, J.B., Brown, R.A., and Priestley, J.V. (2010). The neuroprotective effects of fibronectin mats and fibronectin peptides following spinal cord injury in the rat. Neuroscience 168, 523–530.
44. Tate, C.C., Shear, D.A., Tate, M.C., Archer, D.R., Stein, D.G., and LaPlaca, M.C. (2009). Laminin and fibronectin scaffolds enhance neural stem cell transplantation into the injured brain. Journal of tissue engineering and regenerative medicine 3, 208–217.
45. Tate, C.C., Garcia, A.J., and LaPlaca, M.C. (2007). Plasma fibronectin is neuroprotective following traumatic brain injury. Exp. Neurol. 207, 13–22.
46. Sakai, T., Johnson, K.J., Murozono, M., Sakai, K., Magnuson, M.A., Wieloch, T., Cronberg, T., Isshiki, A., Erickson, H.P., and Fassler, R. (2001). Plasma fibronectin supports neuronal survival and reduces brain injury following transient focal cerebral ischemia but is not essential for skin-wound healing and hemostasis. Nat. Med. 7, 324–330.
47. Tang, X., Davies, J.E., and Davies, S.J. (2003). Changes in distribution, cell associations, and protein expression levels of NG2, neurocan, phosphacan, brevican, versican V2, and tenascin-C during acute to chronic maturation of spinal cord scar tissue. J. Neurosci. Res. 71, 427–444.
48. Camand, E., Morel, M.P., Faissner, A., Sotelo, C., and Dusart, I. (2004). Long-term changes in the molecular composition of the glial scar and progressive increase of serotoninergic fibre sprouting after hemisection of the mouse spinal cord. Eur. J. Neurosci. 20, 1161–1176.
49. Perkins, M.E., Ji, T.H., and Hynes, R.O. (1979). Cross-linking of fibronectin to sulfated proteoglycans at the cell surface. Cell 16, 941–952.
50. Lewandowska, K., Choi, H.U., Rosenberg, L.C., Zardi, L., and Culp, L.A. (1987). Fibronectin-mediated adhesion of fibroblasts: inhibition by dermatan sulfate proteoglycan and evidence for a cryptic glycosaminoglycan-binding domain. J. Cell Biol. 105, 1443–1454.
51. Isemura, M., Sato, N., Yamaguchi, Y., Aikawa, J., Munakata, H., Hayashi, N., Yosizawa, Z., Nakamura, T., Kubota, A., Arakawa, M., et al. (1987). Isolation and characterization of fibronectin-binding proteoglycan carrying both heparan sulfate and dermatan sulfate chains from human placenta. J. Biol. Chem 262, 8926–8933.
52. Noble, L.J. and Wrathall, J.R. (1989). Distribution and time course of protein extravasation in the rat spinal cord after contusive injury. Brain Res. 482, 57–66.
53. Whetstone, W.D., Hsu, J.Y., Eisenberg, M., Werb, Z., and Noble-Haeusslein, L.J. (2003). Blood-spinal cord barrier after spinal cord injury: relation to revascularization and wound healing. J. Neurosci. Res. 74, 227–239.
54. Metz, G.A., Curt, A., van de Meent, H., Klusman, I., Schwab, M.E., and Dietz, V. (2000). Validation of the weight-drop contusion model in rats: a comparative study of human spinal cord injury. J. Neurotrauma 17, 1–17.

Address correspondence to:
Jae K. Lee, PhD
University of Miami School of Medicine
Miami Project to Cure Paralysis
Department of Neurological Surgery
1095 NW 14th Terrace, LPLC 4-19
Miami, FL 33136

E-mail: JLee22@med.miami.edu